PERGAMON

AVAILABLE AT
www.ComputerScienceWeb.com
POWERED BY SCIENCE DIRECT®

Neural Networks 16 (2003) 649–656

Neural Networks

www.elsevier.com/locate/neunet

2003 Special issue

Pattern completion through phase coding in population neurodynamics

A. Gutierrez-Galvez, R. Gutierrez-Osuna*

Department of Computer Science, Texas A & M University, College Station, TX 77843-3112, USA

Abstract

This article presents an alternative phase coding mechanism for Freeman's KIII model of population neurodynamics. Motivated by experimental evidence that supports the existence of a neural code based on synchronous oscillations, we propose an analogy between synchronization in neural populations and phase locking in KIII channels. An efficient method is proposed to extract phase differences across granule channels from their state-space trajectories. First, the scale invariance of the KIII model with respect to phase information is established. The phase code is then compared against the conventional amplitude code in terms of their bit-wise and across-fiber pattern recovery capabilities using decision-theoretic principles and a Hamming-distance classifier. Graph isomorphism in the Hebbian connections is exploited to perform an exhaustive evaluation of patterns on an 8-channel KIII model. Simulation results show that phase information outperforms amplitude information in the recovery of incomplete or corrupted stimuli.

Keywords: Olfactory system; KIII model; Neural coding; Coherent oscillation; Associative memory

1. Introduction

Neural coding schemes based on firing synchrony are the most compelling hypothesis for a temporal code spatially distributed across large neural populations. These types of codes have been found experimentally in different neocortical areas (Recce, 2001), and play an important role in the integration of visual information (Singer & Gray, 1995) and the codification of odors (Laurent & Davidowitz, 1994; MacLeod & Laurent, 1996). The objective of this paper is to ascertain whether this coding mechanism can be exploited in the KIII model of Freeman and colleagues (Chang, Freeman, & Burke, 1998a; Yao & Freeman, 1990), arguably the most complete neurodynamics model of the olfactory system.

The long term goal of this work is to develop biologically-plausible computational models to process data from chemical sensor arrays, commonly referred to as the electronic nose. An e-nose consists of (1) an array of chemical sensors with broad and overlapping selectivities and (2) a pattern recognition engine capable of associating sensor patterns with the corresponding odor labels (Gardner & Bartlett, 1999). Biologically-inspired approaches have been the focus of attention in recent years (Pearce, 1997) as an alternative to the statistical pattern recognition procedures commonly employed in e-nose data processing (Gutierrez-Osuna, 2002).

Along these lines, our experience with the KIII model (Gutierrez-Osuna & Gutierrez-Galvez, 2002; Gutierrez-Osuna & Sun, 2002) shows that the information provided by the amplitude of the channels tends to degrade when the input patterns have a significant level of overlap, as is oftentimes the case in electronic nose data due to the cross-selectivity of the chemical sensors. This raises the question whether additional robust information can be extracted from the output of the model. In particular, we have observed that the KIII has a tendency to display similar phases in channels that encode for the same odor. This observation, along with experimental evidence for a neural code based on coherent oscillations in neural populations, motivates the study presented in this paper.

2. Temporal coding and coherent oscillations

Work by Adrian (Adrian, 1926, 1928) more than 75 years ago showed that the firing rate of stretch receptor neurons is related to the force being applied to the muscles. This seminal contribution led to the widespread belief that firing rate was the code used by neural systems to transmit information. As a consequence, early neural network models interpreted the output of artificial neurons as an

* Corresponding author. Tel.: +1-979-845-2942; fax: +1-979-847-8578.
E-mail address: rgutier@cs.tamu.edu (R. Gutierrez-Osuna).

0893-6080/03/$ - see front matter © 2003 Elsevier Science Ltd. All rights reserved.
doi:10.1016/S0893-6080(03)00107-2

abstraction of the neural firing rate in their biological counterparts. In recent years, this view has been challenged with ample experimental evidence showing the need to take into consideration the temporal dimension in neural information processing.

Undisputable evidence for a temporal code is best illustrated by the work of Thorpe et al. (van Ruellen & Thorpe, 2000; Thorpe, Delorme, & Van Ruellen, 2001), who have shown that humans and monkeys are able to respond to a visual categorization problem in a very short period of time. In their experiments, an image is briefly flashed and the subject has to decide if it belongs to a target category or not. Considering (i) the pathway of the visual signal as it propagates through the brain, (ii) the minimum time required for a neuron to generate an action potential and (iii) the response time of the subjects in these experiments, it is possible to determine that there is time for only one spike to be generated at every relay station in the visual pathway. This result clashes with a frequency-rate coding hypothesis, and clearly points to the existence of a temporal dimension.

A number of possible temporal coding mechanisms have been proposed, including inter-spike interval codes, time of arrival (latency) codes and synchrony codes (Cariani, 1995). Among these, the synchronous oscillation of ensembles presents the most compelling empirical evidence. Synchronization has been proposed as a potential mechanism to correlate information from different senses or different parts of the brain (Recce, 2001). It has also been found to play a role in visual feature integration (Singer & Gray, 1995). Of particular interest to our work, Laurent et al. (Laurent & Davidowitz, 1994; MacLeod & Laurent, 1996) have found that synchronous oscillations of neuron populations in insects is used as an odor encoding mechanism. Their work has shown that different odors evoke coherent oscillations in different but usually overlapping ensembles of neurons in the olfactory system.

3. The KIII model

The KIII is a neurodynamics model of the olfactory system developed by Freeman and colleagues (Chang et al., 1998a; Yao & Freeman, 1990) over the last 30 years. The output of the model reproduces electroencephalographic (EEG) recordings in the olfactory system by modeling the oscillatory behavior of neuron populations. The topology of the KIII, shown in Fig. 1, is based on the physiological structure of the mammalian olfactory system. Each node in the KIII represents a population of neurons, modeled by a second order differential equation, and each edge models the interaction between two populations. The strength of this interaction is controlled by a weight, which is positive when the connection is excitatory and negative if the connection is inhibitory.

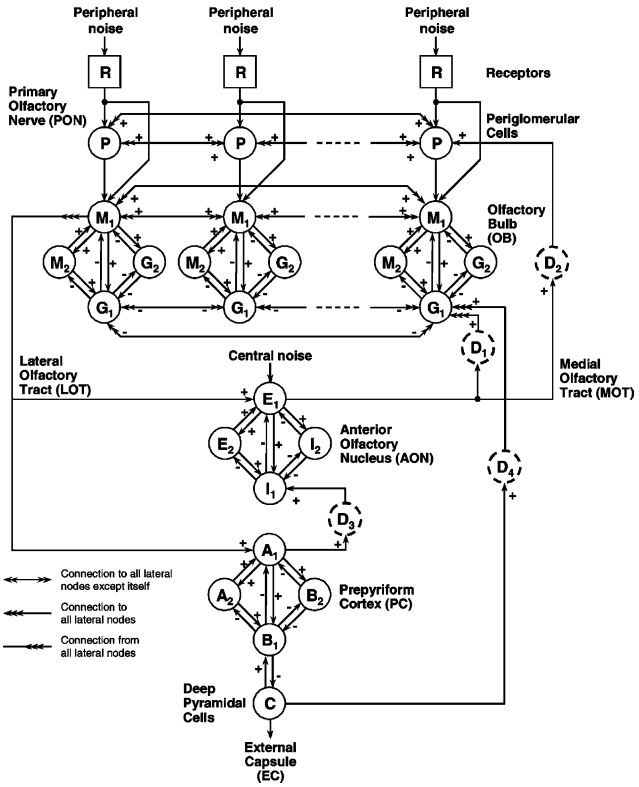

Fig. 1. Structure of the KIII model (from Chang et al., 1998b).

Odor stimuli are presented to the system as patterns, generally binary, through an input layer of receptors. Each receptor is connected to a periglomerular cell and a set of two mitral and two glomerular ensembles, forming a channel. Each of these channels can then be associated with one bit of the binary input stimulus and the corresponding output pattern. The KIII is able to store previously seen patterns by means of Hebbian lateral connections at the M1 mitral layer. This allows the model to work as an associative memory for recovering incomplete or corrupted stimuli.

In the absence of an external stimulus, the KIII channels follow an aperiodic oscillatory behavior known as a basal state. When an input is presented, the system moves into a global attractor in state space, which can also be observed as pseudo-periodic oscillations in the output channels. The amplitude of the oscillations at each channel depends on the activation level of its receptor input, but is also influenced by other receptors as a result of the Hebbian lateral connections. The output pattern of the KIII is commonly assumed to be encoded in the amplitude or RMS of the oscillations of each channel (Yao, Freeman, Burke, & Yang, 1991), which does not exploit the temporal dimension of the KIII dynamics. Considering that the KIII is a model of neuron populations, it is appealing to consider the phase of the oscillations across channels as an analogous of the coherent oscillation coding scheme in biological neural systems. Hence, the goal of this paper is to investigate

whether phase information can in fact be used as a coding mechanism and, if so, compare its pattern-recovery performance against the conventional amplitude code.

3.1. Phase coding in the KIII model

In order to efficiently capture phase information, we consider the state-space trajectory of pairs of KIII channels (G1 populations) as a two-dimensional distribution. As shown in Fig. 2, differences in phase (θ) can be mapped into the correlation coefficient (ρ) of the 2D distribution, and vice versa. Two ideal sinusoidal waveforms with the same phase will lead to a correlation coefficient $\rho = 1$ (Fig. 2(a)), whereas a $\theta = 180°$ phase difference result in a correlation coefficient of $\rho = -1$. Intermediate phase differences result in correlation coefficients between those two extremes $[-1,1]$.

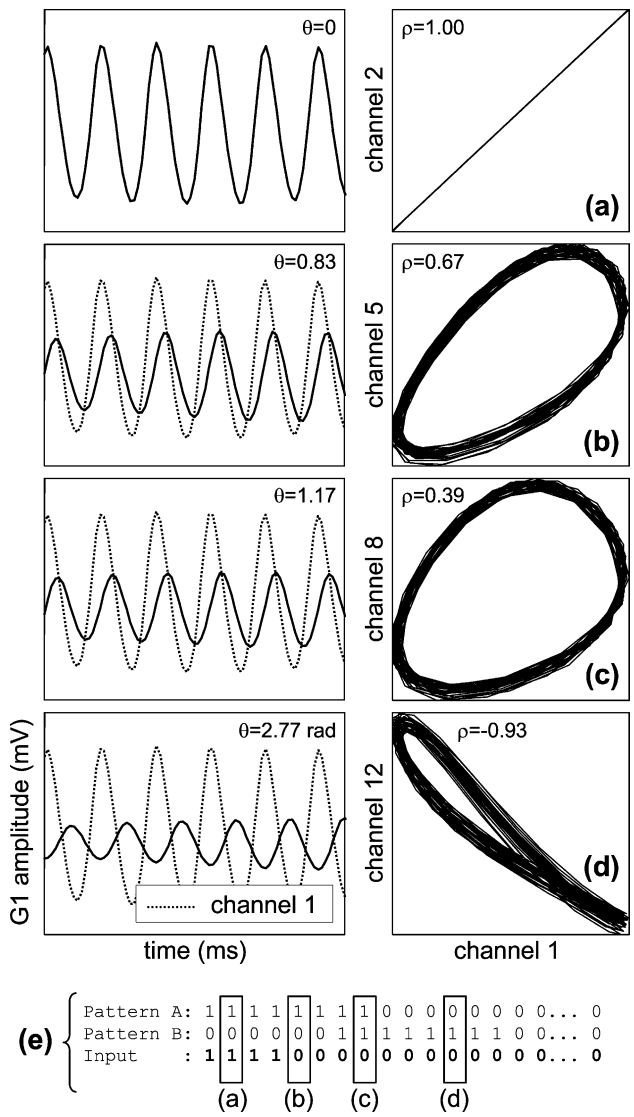

Fig. 2. Extracting phase information from the KIII model.

The waveforms and trajectories in Fig. 2 were obtained by training a 32-channel KIII on two binary patterns, and presenting a distorted version of the first pattern at the inputs. It can be seen that the shape and orientation of the attractors can be associated to different types of errors in the input stimulus. It is also important to note that the correlation coefficient not only captures information about the orientation of the principal eigenvector but also about the area enclosed by the trajectory (i.e. the shape of the attractor).

3.2. KIII implementation

The KIII model with matrix formulation described in Chang, Freeman, & Burke, 1998b was employed in this work. The model was implemented in MATLAB using fourth-order Runge-Kutta ODE integration with a time step of 1.0 ms. Initial conditions for all variables and their derivatives were set to zero. Parameter values for the KIII model are summarized in Table 1. The KIII model presented an aperiodic oscillatory behavior with a $1/f$ power spectra, as shown in Fig. 3 for a 2000 ms simulation of the basal state. Following (Kozma & Freeman, 2001), the more informative part of the signal is located in the gamma frequencies (20–80 Hz). For this reason the G1 signals were band-pass filtered to remove energy outside the gamma band. In what follows, the phase and amplitude are computed on this filtered signal. Comparable results, however, were obtained on the unfiltered signals.

4. Scaling invariance

Invariance of the KIII model with respect to the number of channels has been empirically established (Yao &

Table 1
Parameter values for the KIII model (from (Chang et al., 1998a))

a	0.22	q^C	5.000
b	0.72	w_{M1P}	0.050
q^P	1.824	w^{low}_{M1M1L}	0.599
w_{PPL}	0.900	w^{high}_{M1M1L}	2.100
k_{PR}	0.500	w_{E1M1}	1.311
q^{OB}	5.000	w_{A1M1}	1.710
w_{MM}	1.500	w_{G1G1L}	−0.580
w_{MG}	−2.063	w_{CB1}	−1.543
w_{GM}	2.323	w_{B1C}	0.698
w_{GG}	−2.445	w_{G1D1}	2.349
k_{M1R}	1.000	w_{PD2}	1.087
q^{AON}	5.000	w_{I1D3}	2.553
w_{EE}	1.202	w_{G1D4}	2.305
w_{EI}	−1.426	T^s_1	20.000
w_{IE}	1.372	T^e_1	11.000
w_{II}	−1.571	T^s_2	22.000
q^{PC}	5.000	T^e_2	15.000
w_{AA}	0.823	T^s_3	21.000
w_{AB}	−1.938	T^e_3	12.000
w_{BA}	1.947	T^s_4	30.000
w_{BB}	−2.354	T^e_4	24.000

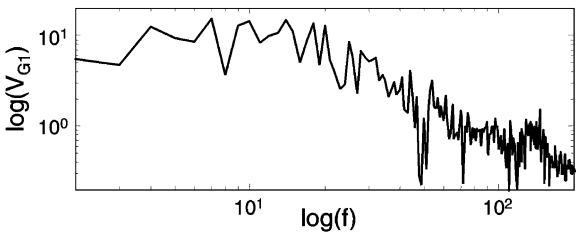

Fig. 3. Power spectra for a 2000 ms simulation of basal state.

Freeman, 1990) in terms of the amplitude and general shape of the oscillations observed at each channel. To determine if these results can be generalized to phase information, we present a thorough study on three KIII models with 16, 32 and 64 channels. The study simulates a two-odor classification problem with varying levels of complexity in terms of (1) the degree of overlap between the two stored patterns and (2) the number of missing or corrupted channels that are presented at the input.

Fig. 4 shows the two input patterns for the 16-channel case. Each pattern consists of four active channels, represented by a 1, and 12 inactive channels, represented by a blank bit. Due to the symmetry of the problem, in what follows the KIII model is always excited with a stimulus from pattern A. To incorporate different degrees of overlap, three patterns sets are considered having 0, 1 and 2 bits of overlap. Each one of these three sets leads to a unique Hebbian associative matrix and, therefore, a separate KIII model. Fig. 4(a) shows the situation where the patterns have an overlap of 2 bits. To simulate incomplete patterns (e.g. caused by sensor degradation), 0, 1 or 2 of the active bits in the stimulus may be set to zero. Fig. 4(b) shows the case where the stimulus for pattern A is incomplete by one bit. Finally, to simulate corrupted patterns (e.g. to due to background odors), 0, 1 and 2 bits not belonging to either pattern may be set to one. Fig. 4(c) shows a stimulus for Pattern A with one corrupted bit. All these different combinations lead to $3 \times 3 \times 3 = 27$ possible scenarios for a 16-channel KIII model. Data for the 32- and 64-channel models is obtained by scaling the stored patterns and input stimuli by a factor of 2 and 4, respectively.

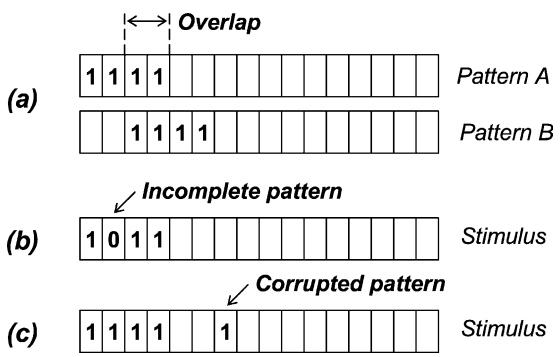

Fig. 4. Overlap between input patterns for a 16-channel KIII (a). Simulating an incomplete (b) and a corrupted (c) input pattern.

Simulation results are presented in Fig. 5 in the form of bi-variate scatter plots. Each point in the scatter plots represents the output of one KIII channel for one stimulus. The abscissa axis is the RMS amplitude of the channel, whereas the ordinate axis is the phase relative to channel 0, which is consistently activated and used as a reference. Four different cases of input-stimulus → desired-response are

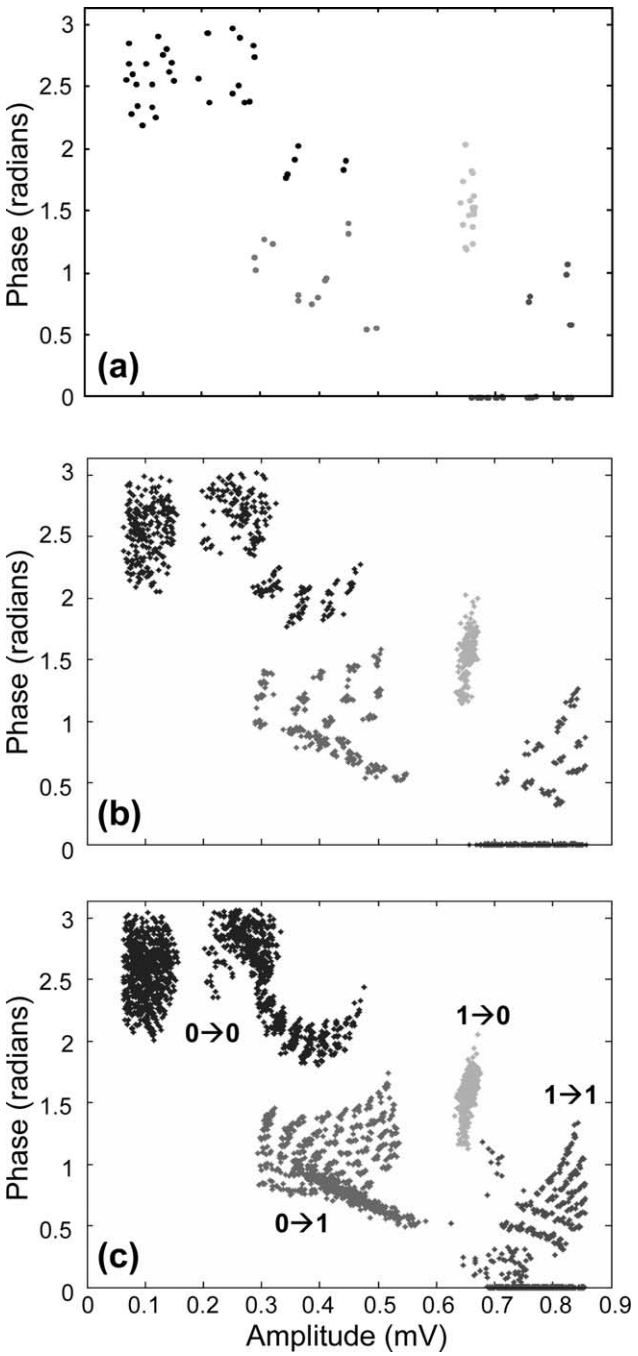

Fig. 5. Scatter plot of amplitude vs. phase codes for different input-stimulus → desired-response cases.

considered in the study, which correspond to two correct and two erroneous input stimuli:

- 1 → 1 (no error): stimulus in a channel that encodes for pattern A;
- 0 → 0 (no error): no stimulus in a channel that does not encode for pattern A;
- 0 → 1 (incomplete pattern): missing stimulus in channel that encodes for pattern A;
- 1 → 0 (corrupted pattern): noisy stimulus in a channel that does not encode for pattern A;

The results in Fig. 5 show that, although a higher number of channels yields a more detailed structure of the amplitude/phase clusters, these scatter plots have a similar structure regardless of the number of channels. This result leads to the conclusion that the KIII model is not only scale invariant with respect to amplitudes, a result previously established in Yao & Freeman, 1990, but also with respect to phase information.

4.1. Bit recovery

An important conclusion can also be extracted from these scatter plots. Fig. 6 shows the marginal univariate distribution of the amplitude and phase codes in the 64-channel model for each of the four input-stimulus → desired-response cases. A Gaussian distribution has been assumed for visualization purposes. It can be observed that the amplitude code is able to recover either incomplete or corrupted bits, but not both, since the 0 → 1 and 1 → 0 densities lie on opposite sides of their desired response. This result indicates that the amplitude of a particular channel tends to be driven primarily by the input stimulus rather than by the lateral connections in the Hebbian matrix. In the case of a phase code, a simple threshold can be obtained to correct the majority of the incomplete or corrupted bits, indicating a higher sensitivity to lateral connections. Bit recovery is, therefore, more reliable using phase information.

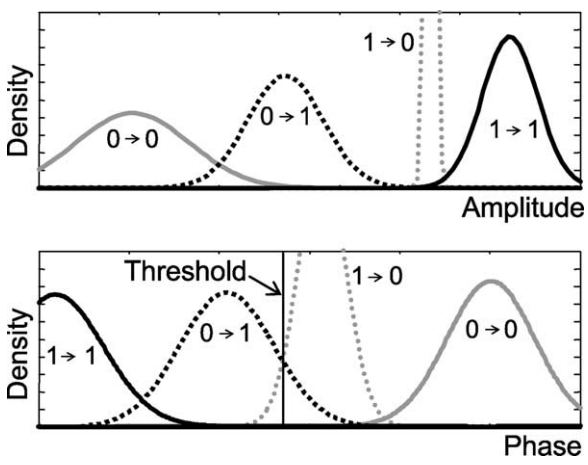

Fig. 6. Univariate density functions for the amplitude and phase codes.

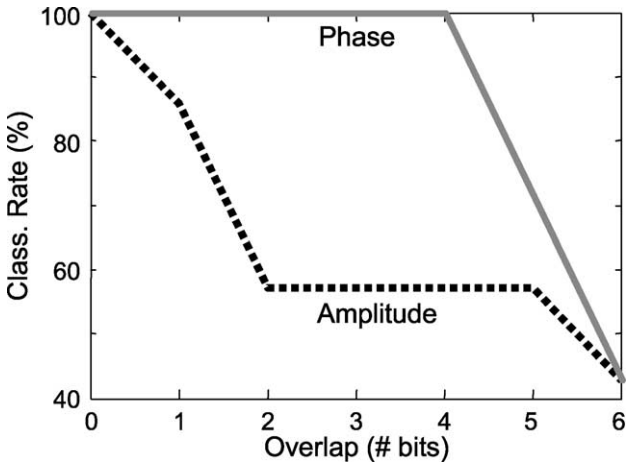

Fig. 7. Performance of a Hamming-distance classifier on the two codes.

4.2. Pattern recovery: preliminary results

The results in the previous sections demonstrate the significant advantage of a phase code in the recovery of individual errors at the channel level (bit-wise). How do these results translate into classification performance at the across-fiber pattern level? To explore this issue, a Hamming-distance classifier (Lippmann, 1987) was employed at the output of the KIII. Oscillatory activity (phase or amplitude) at each KIII output channel was binarized in a decision-theoretic manner with a Likelihood Ratio Test (van Trees, 1968), where the threshold was obtained by assigning 0 → 0 and 1 → 0 bits into one Gaussian density, and 1 → 1 and 0 → 1 bits into the second one. Inputs and prototype patterns were generated using a 16-channel KIII model with 8 active channels (as opposed to the 4 active channels in Fig. 4) to explore higher levels of overlap between patterns. The number of incomplete or corrupted bits was allowed to range between 0 and 2.

The average classification rate as a function of prototype overlap is shown in Fig. 7, where ties (the input pattern is equidistant from the two prototypes) are counted as miss-classifications. With zero overlap between the two prototypes (1111111100000000 and 0000000011111111), both codes provide 100% classification rate since the Hamming-distance classifier is robust against errors in a few bits. As the overlap between the prototypes grows, discrimination between them becomes more difficult. As a result, bit-wise corrections become increasingly relevant, allowing the phase code to clearly outperform amplitude information.[1]

[1] Not shown in the figure, for overlaps of 7 bits (1111111100000000 and 0111111110000000) and 8 bits (the two prototypes are identical), the performance of both codes drops to 0%.

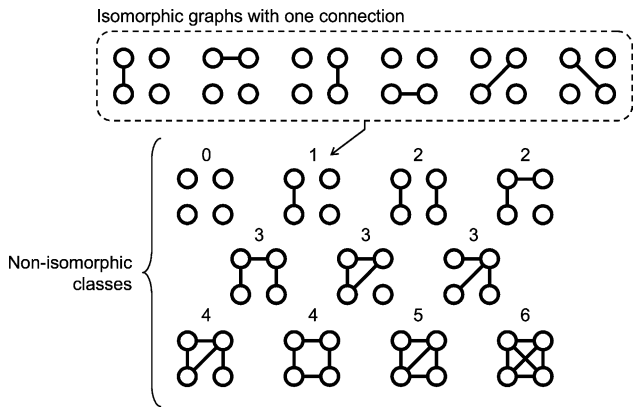

Fig. 8. Reduction of a 4-channel model to 11 non-isomorphic classes. The index above each graph denotes the number of active Hebbian connections.

5. Symmetry of the associative memory matrix

Once the scale invariance of the KIII model with respect to phase information has been validated, the study can now be focused on a lower dimensional model where an exhaustive evaluation of every possible combination of input stimulus and pattern sets is computationally feasible. Although 2- and 4-channel models could be used to this effect, the results in Fig. 5 show that more channels lead to higher resolution. For this reason, an 8-channel model is chosen for the final study.

In order to avoid exploring redundant combinations, the symmetries in the KIII associative-memory matrix will be exploited. Following Yao & Freeman, 1990, the mitral–mitral lateral connections can be computed as:

$$W_{\mathrm{M1}} = \sum_{\forall i} f(p_i p_i^T) \tag{1}$$

where p_i is the correct input pattern for the ith odor class, and $f(\cdot)$ is a threshold function so that the elements in W_{M1} are binary, either HIGH or LOW[2] (diagonal elements in the matrix are set to zero.) Thus, a HIGH element in the Hebbian matrix represents two KIII channels that are simultaneously active for *at least* one odor pattern. Since different pattern sets can lead to the same Hebbian matrix, an exhaustive evaluation of every possible pattern set can be reduced to the study of all possible matrix configurations.

A representation of the Hebbian matrix as an undirected graph will be used to illustrate the existing symmetries. For simplicity, assume a 4-channel model with only one connection between channels. Since the channels are symmetric, the behavior of the system will be the same regardless of where this connection is located, as shown in Fig. 8. Generalizing this idea, graphs with the same number of connections and the same topology (i.e. isomorphic graphs) have to be considered just once. As a result, a 4-channel model with $2^6 = 64$ possible configurations is reduced to the 11 non-isomorphic graphs in Fig. 8. Similarly, a 8-channel model can be reduced from $2^{28} = 2.7 \times 10^8$ to 1192 cases, for a significant savings in CPU time.

6. Pattern recovery: final results

The final comparison of the two coding schemes will be performed on an 8-channel KIII model, for a total of 1192 non-isomorphic cases. As opposed to the preliminary study in Section 4.1, where performance was studied as a function of degrees of overlap in the pattern set and distortions in the input stimulus, the pattern recovery capabilities in this final study can only be evaluated in terms of the properties of each graph since the relationship between pattern sets and graphs is many-to-one. Two observations will greatly simplify this analysis. First, any two neighboring nodes (those that are connected directly by an edge) represent channels that are simultaneously active for at least one stored pattern. Conversely, any two nodes that are more than one edge away represent channels where two or more patterns overlap. Therefore, it is possible to analyze the across-fiber pattern-recovery performance of the phase and amplitude codes by comparing the activation between nodes connected by a single edge (which represents a true pattern) against the activation between nodes connected by a multi-edge path (which represents an undesirable overlap).

This idea is shown in Fig. 9(a). For a given graph, a single input stimulus is applied to the channel with the highest number of lateral connections (d_0 in the figure), and the activity on the remaining channels is analyzed. Nodes within one edge from d_0 (denoted by d_1) are part of a pattern. Nodes two edges away (denoted by d_2) are the effect of an overlap between two or more patterns. The remaining

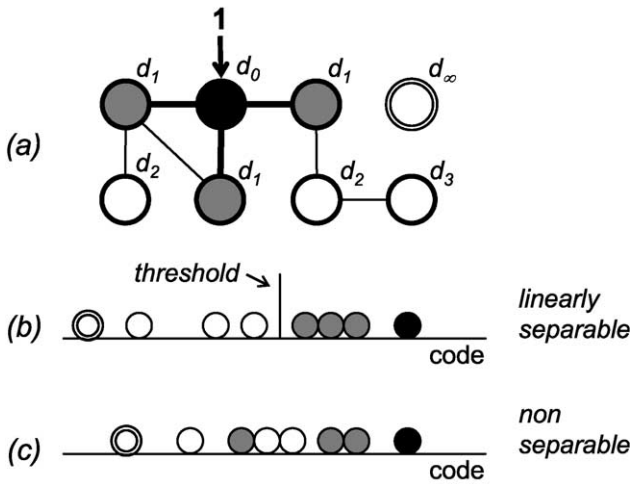

Fig. 9. (a) Pattern and overlap bits for a given Hebbian graph. (b,c) Pattern recovery as a linear separability problem.

[2] LOW and HIGH values are denoted by $W^{\mathrm{low}}_{\mathrm{M1M1L}}$ and $W^{\mathrm{high}}_{\mathrm{M1M1L}}$, respectively, in Table 1.

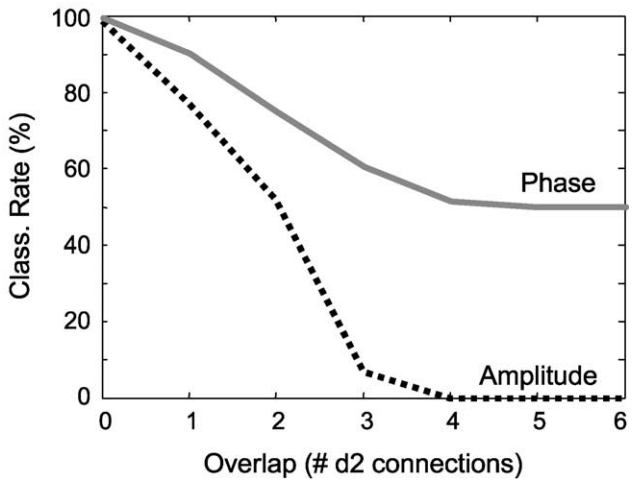

Fig. 10. Overall performance of the phase and amplitude codes as a function of pattern overlap.

nodes (d_3 through d_∞) can be neglected since they involve higher-order overlaps between patterns. Fig. 9(b) shows the situation where the response of d_0 and d_1 nodes is linearly separable from the rest, indicating that a simple threshold function could be used to recover an incomplete pattern from an input stimulus having a single active channel. Fig. 9(c) shows the opposite situation, where the response of d_0 and d_1 nodes is not linearly separable from the rest and, as a result, the incomplete pattern cannot be recovered.

The procedure outlined in Fig. 9 is repeated individually for each of the 1192 non-isomorphic cases in the 8-channel KIII in order to measure the pattern recovery capabilities of the amplitude and phase codes. The results are presented in Fig. 10 as a function of the number of d_2 connections in each graph, which can be related to the overlap (e.g. the complexity) of the corresponding pattern sets. Each point in the plot represents the percentage of graphs where

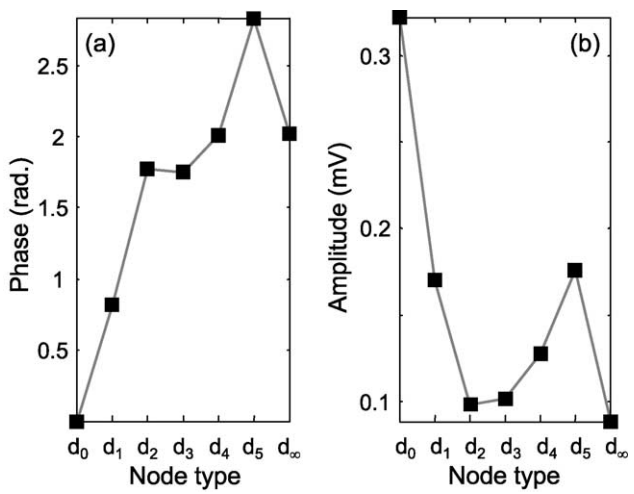

Fig. 11. Phase difference and amplitude as a function of distance (number of edges) to the input node.

the linear separability in Fig. 9(b) is achieved, relative to the total number of graphs. This result shows that the performance of the amplitude code decreases dramatically as the degree of overlap increases, whereas the phase code degrades in a more graceful manner and always provides higher classification rates.

The average phase difference between the input node (d_0) and all remaining nodes is shown in Fig. 11(a). The phase of d_1 nodes is closer to the input node than to the remaining nodes. For comparison, the corresponding average amplitudes are shown in Fig. 11(b). In this case the situation is reversed, with the amplitude of d_1 nodes being farther from the input node than to the other nodes. These results provide additional evidence for the superiority of the phase code.

7. Conclusions

This article has proposed an analogy between coherent oscillations in neural populations and phase locking in the KIII model. We have shown that phase differences between channels can be efficiently captured by treating the state-space trajectory as a two-dimensional distribution and computing its correlation coefficient. Scale invariance of the KIII with respect to this phase information has been empirically validated on three models with 16, 32 and 64 channels. The performance of the phase code has been demonstrated in terms of (1) bit-wise error recovery from a decision-theoretic viewpoint and (2) across-fiber pattern completion with a Hamming-distance classifier.

An exhaustive comparison of the pattern recovery capabilities of the proposed phase coding and the conventional amplitude coding has been presented on an 8-channel model. In order to avoid a combinatorial explosion, redundant pattern and stimulus combinations have been eliminated by means of graph isomorphism. Experimental results show that information embedded in the phase of the KIII channels clearly outperforms the amplitude code.

The present study has focused on binary stimuli, but the KIII has also been shown (Kozma & Freeman, 2001) to work efficiently with continuous inputs. Thus, a natural extension of the work presented in this article is to consider continuous amplitude and phase representations. Additional information other than correlation coefficients (which relate to phase for sinusoidal waveforms) could also be extracted from the KIII dynamic attractors in two- or higher-dimensional state spaces. These areas constitute promising directions for future work.

Acknowledgements

This material is based upon work supported by the National Science Foundation under CAREER Grant No. 9984426/0229598. Ping Sun is acknowledged for earlier work on an implementation of the KIII model.

References

Adrian, E. D. (1926). The impulses produced by sensory nerve ending. *The Journal of Physiology*, *61*, 49–72.

Adrian, E. D. (1928). *The basis of sensation*. New York: Norton.

Cariani, P. (1995). As if time really mattered: temporal strategies for neural coding of sensory information. *Communication and Cognition—Artificial Intelligence*, *12*(1/2), 157–219.

Chang, H., Freeman, J. W., & Burke, B. (1998a). Biologically modeled noise stabilizing neurodynamics for pattern recognition. *International Journal of Bifurcation and Chaos*, *8*(2), 321–345.

Chang, H., Freeman, W. J., & Burke, B. (1998b). Optimization of olfactory model in software to give 1/*f* power spectra reveals numerical instabilities in solutions governed by aperiodic (chaotic) attractors. *Neural Networks*, *11*, 449–466.

Gardner, J. W., & Bartlett, P. N. (1999). *Electronic noses. Principles and applications*. New York: Oxford University Press.

Gutierrez-Osuna, R. (2002). Pattern analysis for machine olfaction: a review. *IEEE Sensors Journal*, *2*(3), 189–202.

Gutierrez-Osuna, R., & Gutierrez-Galvez, A. (2002). Habituation in the KIII olfactory model using gas sensor arrays. *Proceedings of the ninth International Symposium on Olfaction and Electronic Nose* (pp. 171–173). Rome, Italy.

Gutierrez-Osuna, R., & Sun, P. (2002). A biologically-plausible computational architecture for sensor-based machine olfaction. *Proceedings of the ninth International Symposium on Olfaction and Electronic Nose* (pp. 57–59). Rome, Italy.

Kozma, R., & Freeman, W. J. (2001). Chaotic resonance—methods and applications for robust classification of noisy and variable patterns. *International Journal of Bifurcation and Chaos*, *11*(6), 1607–1629.

Laurent, G., & Davidowitz, H. (1994). Encoding of olfactory information with oscillating neural assemblies. *Science*, *265*, 1872–1875.

Lippmann, R. P. (1987). An introduction to computing with neural nets. *IEEE Acoustics, Speech, and Signal Processing Magazine*, 4–22.

MacLeod, K., & Laurent, G. (1996). Distinct mechanisms for synchronization and temporal patterning of odor-encoding neural assemblies. *Science*, *274*, 976–979.

Pearce, T. C. (1997). Computational parallels between the biological olfactory pathway and its analogue 'The Electronic Nose67.

Recce, M. (2001). Encoding information in neuronal activity. In W. Mass, & C. M. Bishop (Eds.), *Pulsed neural networks* (pp. 111–131). Cambridge, MA: MIT Press.

van Ruellen, R., & Thorpe, S. J. (2000). Is it a bird? Is it a plane? Ultra-rapid visual categorization of natural and artifactual objects. *Perception*, *30*, 655–668.

van Trees, H. L. (1968). *Detection, estimation and modulation theory, Part I*. New York: Wiley.

Singer, W., & Gray, C. M. (1995). Visual feature integration and the temporal correlation hypothesis. *Annual Review of Neuroscience*, *18*, 555–586.

Thorpe, S. J., Delorme, A., & Van Ruellen, R. (2001). Spike-based strategies for rapid processing. *Neural Networks*, *14*, 715–725.

Yao, Y., & Freeman, W. J. (1990). Model of biological pattern recognition with spatially chaotic dynamics. *Neural Networks*, *3*, 153–170.

Yao, Y., Freeman, W. J., Burke, B., & Yang, Q. (1991). Pattern recognition by a distributed neural network: An industrial application. *Neural Networks*, *4*, 103–121.